Hindawi
International Journal of Antennas and Propagation
Volume 2022, Article ID 4935681, 8 pages
https://doi.org/10.1155/2022/4935681

Research Article

A Semiblind Receiver for a Two-Way UAV-Aided PIC System Based on the PARAFAC Model

Xi Han,[1] **Yichen Liu**,[2] **Qin Liu**,[2] **Lijun Wang**,[2] **and Zhengping Li**[2]

[1]*Beijing Key Laboratory on Integration and Analysis of Large-Scale Stream Data, School of Information Science and Technology, North China University of Technology, Beijing, China*
[2]*School of Information Science and Technology, North China University of Technology, Beijing, China*

Correspondence should be addressed to Xi Han; jinlucky333@126.com

Received 5 April 2022; Revised 4 November 2022; Accepted 12 November 2022; Published 9 December 2022

Academic Editor: Tao Zhou

In this paper, we consider a two-way communication system using the unmanned aerial vehicle (UAV) as a relay (UAV-aided). This system eliminates impulse interference through an adaptive filter based on the least mean square (LMS) and uses the received signal transmitted by the UAVs to construct a parallel factor (PARAFAC) model. Based on the identifiability condition of the PARAFAC model, a pulse interference cancellation orthogonal pilot tensor (PIC-OPT) receiver without iteration is proposed. Our algorithm is also used in millimeter-wave to achieve the acquisition of channel information. Compared with the least squares method, the simulation results demonstrate the superiority of the proposed semiblind receiver in terms of the relative mean square error and bit error rate.

1. Introduction

With the rapid development of the growing demand for mobile Internet services, two-way communication technology is now widely used in smart metering, security, and load management [1] and has become a research hotspot in the field of modern communications. The use of unmanned aerial vehicles (UAVs) as relays (UAV-aided) for information transmission in the two-way system has gradually come into our field of vision, for their ability to improve spectral efficiency and reduce end-to-end delay and cost [2, 3]. The reliability of signal detection in the two-way UAV-aided system strongly depends on the accuracy of the channel state information (CSI) for all the links involved in the communication process [4].

In two-way communication systems, the main methods to obtain CSI include the autoregressive method [5], the pilot-based channel estimation method [6], and the tensor-based method [7]. In [6], two-channel estimation algorithms, namely the superimposed channel training scheme and the two-stage channel estimation algorithm, were developed for two-way multiple-input multiple-output (MIMO) relay communication systems. In [7], to obtain accurate channel state information, a tensor-based channel estimation algorithm was proposed for two-way MIMO relay systems.

In recent years, tensor-based semiblind receivers have been proposed to solve channel estimation problems with no or only a small number of pilot sequences. The successful application of tensor methods in two-way cooperative systems was proposed in [8–10] using parallel factor (PARAFAC) models. In view of the advantages of tensors in constructing receivers, they can be used to solve the problems of signal and CSI acquisition in two-way UAV-aided communication systems.

In this paper, a two-way UAV-aided cooperative communication system with pulse interference cancellation (PIC) is considered. The signals are transmitted in two stages: first, the two users send signals to the UAVs as relays, and second, the received signals are amplified and forwarded to both users, and the two users still send information to the relay. Pulse interference is introduced in the transmission and needs to be eliminated first. Then, a PIC orthogonal pilot tensor (PIC-OPT) receiver is proposed to be used to obtain

accurate CSI. Compared with other iterative receivers, such as alternating least squares (ALS) receivers and minimum mean square error (MMSE) receivers, the proposed receiver has lower complexity and requires no iteration. Simulation results show the superiority of the PIC-OPT receiver in terms of the relative mean square error (rMSE).

1.1. Notations. Column vectors, matrices, and tensors are denoted by boldface lower-case (x), bold-face capital (X), and calligraphic ($\mathcal{X}$) letters, respectively. X^T, $\mathrm{X}^\dagger$, and X^{-1} are the transpose, the pseudoinverse, and the inverse, respectively. $\widehat{\mathrm{A}}$ represents the estimation of A. The diag(a) operator forms a diagonal matrix by putting the vector a on its main diagonal. $\circ$, $\otimes$, and $\odot$ denote the outer, the Kronecker, and the Khatri–Rao matrix products, respectively.

2. Two-Way UAV-Aided PIC Cooperative Communication System

A two-way UAV-aided cooperative communication system is considered, as illustrated in Figure 1. In this system, two sensors and R UAVs are assumed to be users and relays, respectively, with M_1, M_2, and M_r antennas. The signals may be attenuated in the channel, and other disturbances may be introduced. The entire transmission process can be divided into two phases. In the first phase, the users need to send their own information to the relays. In the second phase, the relays amplify and forward the information received in the first phase to the users. The information sent to relays is represented by matrices $\mathrm{X}_1 \in \mathbb{C}^{M_1 \times N_p}$ and $\mathrm{X}_2 \in \mathbb{C}^{M_2 \times N_p}$ where N_p is the pilots' length. The channel matrices between the users and the UAVs are represented by $H_1 \in \mathbb{C}^{M_r \times M_1}$ and $\mathrm{H}_2 \in \mathbb{C}^{M_r \times M_2}$, respectively. The matrix $\mathrm{r} \in \mathbb{C}^{M_r \times N_p}$ is the signal received by the relays, with the additive noise vectors $\mathrm{n}_R \in \mathbb{C}^{M_r \times 1}$ at the relay station. The signals received by the relays can be written as follows:

$$\mathrm{r} = \mathrm{H}_1\mathrm{X}_1 + \mathrm{H}_2\mathrm{X}_2 + n_R. \tag{1}$$

In the second phase, the relays amplify and transmit signals to the users. It is assumed that the channel has reciprocity in this system. Therefore, the signals received by the two users can be expressed as follows:

$$\begin{aligned} \mathcal{Y}_{1w} &= \mathcal{C} \times_1 \mathrm{H}_1^T \times_2 \mathrm{r} + \mathcal{W}_1 + \mathcal{N}_1, \\ \mathcal{Y}_{2w} &= \mathcal{C} \times_1 \mathrm{H}_2^T \times_2 \mathrm{r} + \mathcal{W}_2 + \mathcal{N}_2, \end{aligned} \tag{2}$$

where $\mathcal{W}_1$ and $\mathcal{W}_2$ are the pulse interference, with the noise $\mathcal{N}_1$ and $\mathcal{N}_2$, and $\mathcal{C}$ is the coding matrix. In this situation, an adaptive filter is proposed to eliminate pulse interference, as shown in Figure 2. The least mean square (LMS) is the most common adaptive filtering algorithm in real life. The principle of LMS is to minimize the system output by constantly adjusting the weight of the finite impulse respond (FIR) filter. This method can eliminate the correlation linear weight of the received signal and the reference signal. The structure of the adaptive filter is shown in Figure 3 and the specific steps of the LMS algorithm are shown in Table 1. For example, our input signal is $\mathcal{Y}_{1w}$, which is the sum of the transmitted signal $\mathcal{Y}_1$ and the pulse interference $\mathcal{W}_1$. $\mathcal{W}_r$, the interference sampling of interference source, is another pulse interference related to $\mathcal{W}_1$. The adaptive filter adjusts its own parameters so that the output $y(n)$ at a time n is the best estimate of $\mathcal{W}_1$. $w(n)$ represents the filter weighting coefficient obtained by the adaptive algorithm at time n. The error signal $e(n)$ is the difference between $y(n)$ and the input signal, which means $e(n)$ is the best estimate of the useful signal. Therefore, the output of the system is the useful signal obtained by filtering. In Table 1, $X(n) = [x(n), x(n-1), \ldots, x(n-L+1)]$, and $W(n) = [w(n), w(n-1), \ldots, w(n-L+1)]$ are the actual input vector and filter weight coefficient vector, respectively. L is the filter length, u is the fixed step. The convergence condition of the algorithm is that the step factor u satisfies the following:

$$0 < u < \frac{1}{\boldsymbol{\lambda}_{\max}}, \tag{3}$$

where $\lambda_{\max}$ is the maximum eigenvalue of the autocorrelation matrix of the input signal of the adaptive filter. The adaptive filter can achieve a cancellation amplitude of 20 dB [11, 12]. The hardware circuit design is divided into two parts. In the first part, the transmitter sends the baseband signal through the digital-to-analog converter (DAC) and the digital up-conversion, and in the second part, the receiver converts the received signal through the digital down-conversion and the analog-to-digital converter (ADC) into the baseband signal. Because it is disturbed by pulse interference at the receiving end, the adaptive filter is used to eliminate the interference. After interference processing, the received signals can be simplified as follows:

$$\mathcal{Y}_1 = \mathcal{C} \times_1 \mathrm{H}_1^T \times_2 \mathrm{r} + \mathcal{N}_1, \tag{4}$$

$$\mathcal{Y}_2 = \mathcal{C} \times_1 \mathrm{H}_2^T \times_2 \mathrm{r} + \mathcal{N}_2. \tag{5}$$

In order to obtain the channel information at the two user terminals, we make the following definitions:

$$\begin{aligned} \mathrm{H} &= [\mathrm{H}_1, \mathrm{H}_2] \in \mathbb{C}^{M_r \times (M_1 + M_2)}, \\ \mathrm{X} &= \begin{bmatrix} \mathrm{X}_1 \\ \mathrm{X}_2 \end{bmatrix} \in \mathbb{C}^{(M_1 + M_2) \times N_p}. \end{aligned} \tag{6}$$

3. The PIC-OPT Receiver

In this part, the technology of multidimensional matrices is used to solve the channel estimation problem. Through this solution, estimates of H_1 and H_2 can be calculated from training data. First, for the convenience of calculation, we only write the equation without the presence of noise, which achieves an approximate result. In addition, we first obtain the solution for the first user and the solution for the second user is similar.

Initially, a multidimensional matrix [13, 14] $\mathcal{C}$ is considered, with rank M_r. By using the parallel factorization method, $\mathcal{C}$ can be decomposed as follows:

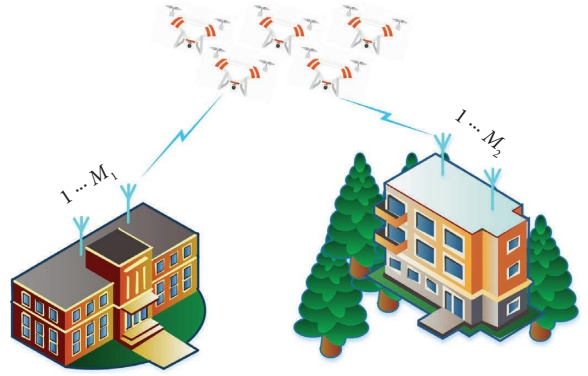

Figure 1: A UAV-aided PIC system.

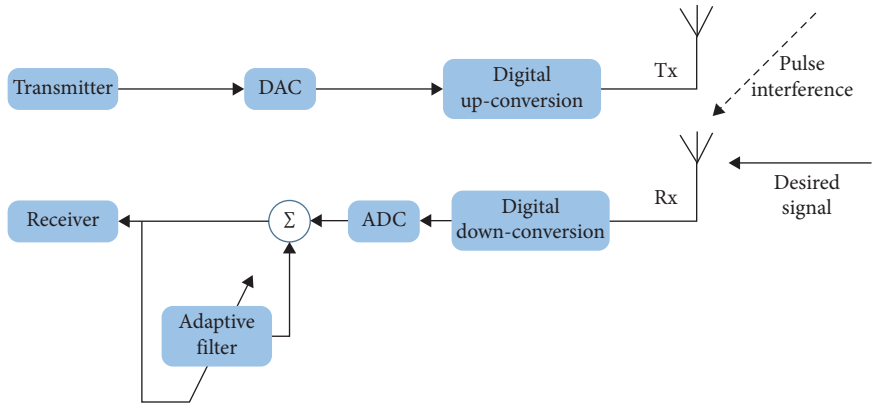

Figure 2: Diagram of pulse interference cancellation.

$$\mathscr{C} = \mathscr{I}_{3,M_r} \times_1 \mathbf{C}_1 \times_2 \mathbf{C}_2 \times_3 \mathbf{C}_3, \tag{7}$$

where $\mathscr{I}_{3,M_r}$ is the multidimensional matrix of size $M_r \times M_r \times M_r$ and the matrices $\mathbf{C}_1, \mathbf{C}_2, \mathbf{C}_3 \in \mathbb{C}^{M_r \times M_r}$ are the factor matrices of this decomposition. In order to reduce the calculation difficulty, we select to deduce the design rules for these factor matrices from the derivation of the channel estimation algorithm instead of the multidimensional matrix $\mathscr{C}$. Inserting (7) into (4), we can get the following:

$$\mathscr{Y}_1 = \mathscr{I}_{3,M_r} \times_1 \left(\mathbf{H}_1^T \mathbf{C}_1\right) \times_2 \left(\mathbf{X}^T \mathbf{H}^T \mathbf{C}_2\right) \times_3 \mathbf{C}_3. \tag{8}$$

According to the slice of the multidimensional matrix [15], the 3-mode unfolding of this matrix can be written as follows:

$$\left[\mathscr{Y}_1\right]_{(3)} = \mathbf{C}_3 \left[\left(\mathbf{H}_1^T \mathbf{C}_1\right) \odot \left(\mathbf{X}^T \mathbf{H}^T \mathbf{C}_2\right)\right]^T. \tag{9}$$

Here, we use elementary properties of the n mode determinant of linear algebra. The Khatri-Rao product $\odot$ can be isolated with the inverted operation of $\mathbf{C}_3$. Therefore, the orthogonal matrix $\mathbf{C}_3$ can be used to isolate the Khatri–Rao product as follows:

$$\left(\mathbf{C}_3^{\dagger} \left[\mathscr{Y}_1\right]_{(3)}\right)^T = \left(\mathbf{H}_1^T \mathbf{C}_1\right) \odot \left(\mathbf{X}^T \mathbf{H}^T \mathbf{C}_2\right). \tag{10}$$

Since $\mathbf{C}_3$ is the orthogonal matrix, the Moore–Penrose pseudo inverse-operation $\mathbf{C}_3^{\dagger}$ causes the Khatri-Rao product in (9) to be measured in reverse per column. Therefore, there must exist matrices $\mathbf{E}_1 \in \mathbb{C}^{M_1 \times M_r}$ and $\mathbf{E}_2 \in \mathbb{C}^{M_2 \times M_r}$ with conditions as shown in [16].

$$\mathbf{E}_1 = \mathbf{H}_1{}^T \mathbf{C}_1, \tag{11}$$

$$\mathbf{E}_2 = \mathbf{X}^T \mathbf{H}^T \mathbf{C}_2. \tag{12}$$

The proposed PIC-OPT receiver as described in Table 2 includes the PIC using an adaptive filter and the singular value decomposition (SVD) of the channel matrices recovery. The computation complexity of the proposed receiver is $M_1^2 N_p + M_1 M_r^3 + M_r^3$.

We design a pilot matrix with orthogonal rows, with the restrictive condition $N_p \geqslant M_1 + M_2$. Additionally, we assume that the pilots transmitted by two users are orthogonal to each other, which can be written as follows:

$$\left(\mathbf{X}_1^T\right)^{\dagger} \mathbf{X}^T = \left[\mathbf{I}_{M_1}, \mathbf{0}_{M_1 \times M_2}\right], \tag{13}$$

$$\left(\mathbf{X}_2^T\right)^{\dagger} \mathbf{X}^T = \left[\mathbf{0}_{M_2 \times M_1}, \mathbf{I}_{M_2}\right]. \tag{14}$$

In consideration of the orthogonality constraint of X, substitute (15) in (13) and we can obtain the following:

$$\tilde{\mathbf{E}}_2 = \left(\mathbf{X}_1^T\right)^{\dagger} \mathbf{E}_2 = \mathbf{H}_2^T \mathbf{C}_2. \tag{15}$$

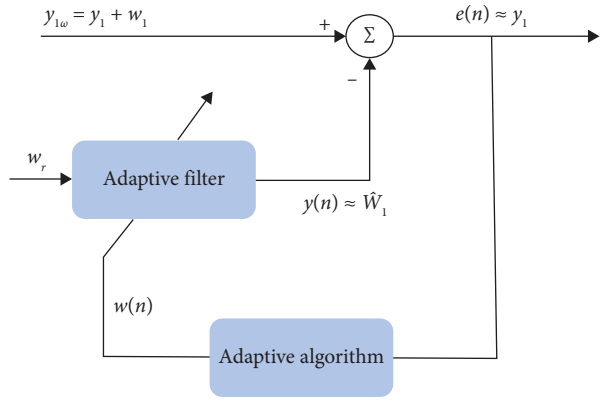

Figure 3: The structure of the adaptive filter.

Table 1: The LMS algorithm.

Step 1: initialize parameters and the initial value of the adaptive filter weighting coefficient $W(0)$. The order and step value are set as M and u, respectively
Step 2: calculate the output result of the filter estimation $y(n) = \mathbf{W}^T(n)X(n)$
Step 3: calculate the error of the filter $e(n) = \mathcal{Y}_{1\omega} - y(n)$
Step 4: the filter weighting coefficient is updated to $w(n+1) = w(n) + 2u\,e(n)X(n)$
Step 5: repeat steps 2–4 above until the weight coefficient of the filter approaches the best filter

Table 2: The PIC-OPT receiver.

Step 1: use the LMS adaptive filter to eliminate the pulse interference, which could eliminate the correlation linear weight of the signal
Step 2: joint estimation of E_1 and E_2
2.1 according to (11)–(13), we set $\Psi \approx E_1 \odot E_2$; the mth column can be obtained as $\Psi_m \approx e_{1,m} \otimes e_{2,m}$
2.2 recast the mth column vector Ψ as the matrix $\widetilde{\Psi}_m \approx e_{2,m}\mathbf{e}_{1,m}{}^{\mathrm{T}} \in \mathbb{C}^{N_p \times M_1}$
2.3 set $m = 1$
2.4 $m \leftarrow m+1$
2.5 compute the SVD as $\widetilde{\Psi}_m = \mathbf{U}_m \Sigma_m \mathbf{V}_m{}^H$
The best rank-one approximation of $\widetilde{\Psi}_m$ in the Fibonacci norm is obtained by $\hat{\mathbf{e}}_{1,m} = \sqrt{\sigma_1}\mathbf{v}_{1,m}^*, \hat{\mathbf{e}}_{2,m} = \sqrt{\sigma_1}\mathbf{u}_{1,m}$
Where σ_1 is the largest singular value, and $u_{1,m}$ and $v_{1,m}$ are the first columns of U_m and V_m, respectively
2.6 go to 2.4 until $m = M_r$
Step 3: calculate the estimates of H_1 and H_2

The channel $\mathbf{H}_1$ and $\mathbf{H}_2$ can be estimated as follows:

$$\begin{aligned} \mathbf{E}_1\mathbf{C}_1^{\dagger} &= \mathbf{H}_1^T, \\ \widetilde{\mathbf{E}}_2\mathbf{C}_2^{\dagger} &= \mathbf{H}_2^T. \end{aligned} \tag{16}$$

According to the uniqueness theorem of PARAFAC model decomposition, (8) is decomposed to obtain unique $\mathbf{E}_1$ and $\mathbf{E}_2$, then the Kruskal rank of the three-factor matrices in the PARAFAC model satisfies the following [17]:

$$k_{\mathbf{E}_1} + k_{\mathbf{E}_2} + k_{\mathbf{C}_3} \geqslant 2M_r + 2, \tag{17}$$

where $k_{\mathbf{E}_1}$ is the Kruskal rank of the matrix $\mathbf{E}_1$ (similarly to $\mathbf{E}_2$ and $\mathbf{C}_3$. In addition, we design the pilot matrix $\mathbf{X}$ with orthogonal rows, with the restrictive condition $N_p \geqslant M_1 + M_2$. It is assumed that $\mathbf{C}_3$ satisfies k rank, and $\mathbf{H}_1$ and $\mathbf{H}_2$ are random matrices, so the factor matrices of the PARAFAC model all satisfy K rank. (20) that can be expressed as follows:

$$M_r + \min\left(M_1, M_r\right) + \min\left(N_p, M_r\right) \geqslant 2M_r + 2. \tag{18}$$

Then, the loading matrices $\mathbf{E}_1, \mathbf{E}_2$, and $\mathbf{C}_3$ are essentially unique up to the permutation and scalar ambiguity, meaning that any other triple $(\hat{\mathbf{E}}_1, \hat{\mathbf{E}}_2, \hat{\mathbf{C}}_3)$ is related to $(\mathbf{E}_1, \mathbf{E}_2, \mathbf{C}_3)$ via

$$\mathbf{E}_1 = \hat{\mathbf{E}}_1\mathbf{\Pi}_1\Delta_1, \mathbf{E}_2 = \hat{\mathbf{E}}_2\mathbf{\Pi}_2\Delta_2, \mathbf{C}_3 = \hat{\mathbf{C}}_3\mathbf{\Pi}_3\Delta_3, \tag{19}$$

where $\Pi \in \mathbb{C}^{M_r \times M_r}$ is the permutation matrix, and $\Delta_i \in \mathbb{C}^{M_r \times M_r}$ $(i = 1, 2, 3)$ is the diagonal scaling matrices satisfying $\Delta_1\Delta_2\Delta_3 = \mathbf{I}_{M_r}$. Considering that the system is a semiblind receiver, the encoding matrix $\mathbf{C}_3$ is known and full rank, so the permutation ambiguity is not considered.

4. Extension in Millimeter Wave MIMO Systems

In the following, we show that the proposed algorithm can also be used to obtain the channel information in millimeter wave MIMO systems. In a downlink millimeter wave MIMO system, the channel matrix in the time domain can be written as follows:

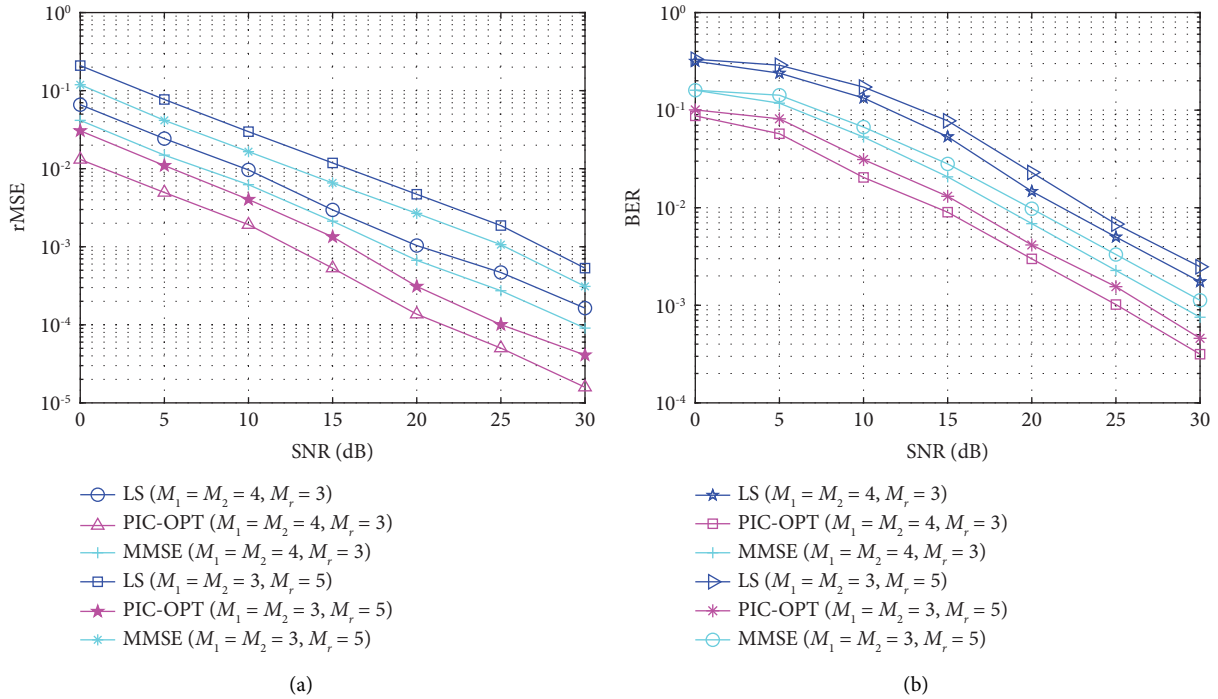

(a) (b)

Figure 4: The rMSE and BER performances of the PIC-OPT algorithm compared with those of the LS algorithm and the MMSE algorithm.

$$\mathbf{H}(\tau) = \sum_{l=1}^{L} \boldsymbol{\alpha}_l \boldsymbol{\alpha}_{MS}(\theta_l) \boldsymbol{\alpha}_{BS}{}^{T}(\varphi_l) \delta(\tau - \tau_l). \tag{20}$$

This mmWave channel model with L scatterers between the user and the base station. τ_l, φ_l, and $\theta_l \in [0, 2\pi]$ represent the time delay, angles of arrival, and departure of a scatter, respectively. $\delta(\cdot)$ is the delta function, α_l is the complex path gain of the l-th path, and $\alpha_{MS}(\theta_l)$ and $\alpha_{BS}(\varphi_l)$ are the antenna array response vectors at the transmitter and the base station. Because of the random distribution of scatterers in space, we assume that different scatterers have different τ_l, and φ_l, as well as $\theta_l \in [0, 2\pi]$. Therefore, we can write the channel matrix $\mathbf{H}_k$ with the kth subcarrier as follows:

$$\mathbf{H}_k = \sum_{l=1}^{L} \boldsymbol{\alpha}_l \exp\left(-j2\pi\tau_l f_s k/\overline{K}\right) \boldsymbol{\alpha}_{MS}(\theta_l) \boldsymbol{\alpha}_{BS}{}^{T}(\varphi_l), \tag{21}$$

where f_s is the sampling rate. In order to obtain $\mathbf{H}_k$ from the received signals, we can construct multidimensional matrices by assuming the digital precoding matrices $\mathbf{F}_k(t)$ and the pilot symbols $\mathbf{S}_k(t)$ remain the same in different subcarriers, which means

$$\mathbf{F}_k(t) = \mathbf{F}(t), \mathbf{S}_k(t) = \mathbf{S}(t), k = 1, \ldots, K. \tag{22}$$

Therefore, the received signals at the kth subcarrier are as follows:

$$\mathbf{Y}_k = \mathbf{Q}_k{}^{T} \mathbf{H}_k \mathbf{P} + \mathbf{W}_k, k = 1, \ldots, K, \tag{23}$$

where $\mathbf{Q_k}$ is comprised of the radio frequency (RF) combining vector $\mathbf{p}(t)$ used at the kth subcarrier, where $\mathbf{p}(t) = \mathbf{F}_{RF}\mathbf{F}(t)\mathbf{S}(t)$ with $t = 1, 2, \ldots, T$, and $\mathbf{F}_{RF}$ is a common RF precoder for all subcarriers. In this way, $\mathbf{Y}_k$ can be deduced as follows:

$$\begin{aligned} \mathbf{Y}_k &= \sum_{l=1}^{L} \tilde{\boldsymbol{\alpha}}_{l,k} \mathbf{Q_k}{}^{T} \boldsymbol{\alpha}_{MS}(\theta_l) \boldsymbol{\alpha}_{BS}^{T}(\varphi_l) \mathbf{P} + \mathbf{W}_k \\ &= \sum_{l=1}^{L} \tilde{\boldsymbol{\alpha}}_{l,k} \tilde{\boldsymbol{\alpha}}_{MS}(\theta_l) \tilde{\boldsymbol{\alpha}}_{BS}^{T}(\varphi_l) + \mathbf{W}_k. \end{aligned} \tag{24}$$

This can be written as a style of multidimensional matrix comprised of vectors.

$$\mathscr{Y} = \sum_{l=1}^{L} \tilde{\boldsymbol{\alpha}}_{MS}(\theta_l)^{\circ} \tilde{\boldsymbol{\alpha}}_{BS}(\varphi_l)^{\circ} e_l + \mathscr{W}, \tag{25}$$

and can be written in the matrix form as follows:

$$\mathscr{Y} = \mathscr{I} \times_1 \mathbf{E} \times_2 \mathbf{B} \times_3 \mathbf{A} + \mathscr{W}, \tag{26}$$

where $\mathbf{E}, \mathbf{B}$, and $\mathbf{A}$ are the factor matrices of this decomposition. Considering the sparse scattering nature of the mmWave channel, L is usually smaller than the dimensions of $\mathscr{Y}$, which means the multidimensional matrix $\mathscr{Y}$ has a low-rank structure, which ensures that the canonical decomposition [16] is unique with scaling and permutation ambiguities. Therefore, we can obtain the estimation parameters $\{\tau_l, \theta_l, \varphi_l, \alpha_l\}$, which construct the mmWave channels by performing a multidimensional matrix decomposition of the received signal $\mathscr{Y}$.

5. Simulation Results

In this section, 5000 Monte Carlo simulations are used to verify the performance of the proposed semiblind receiver.

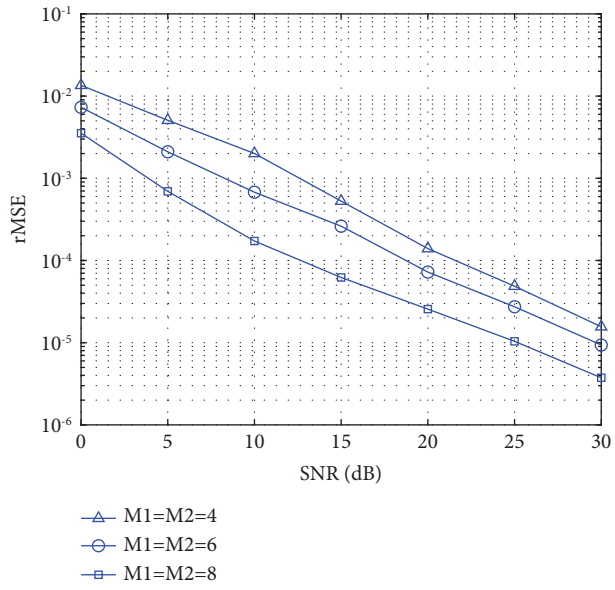

(a)

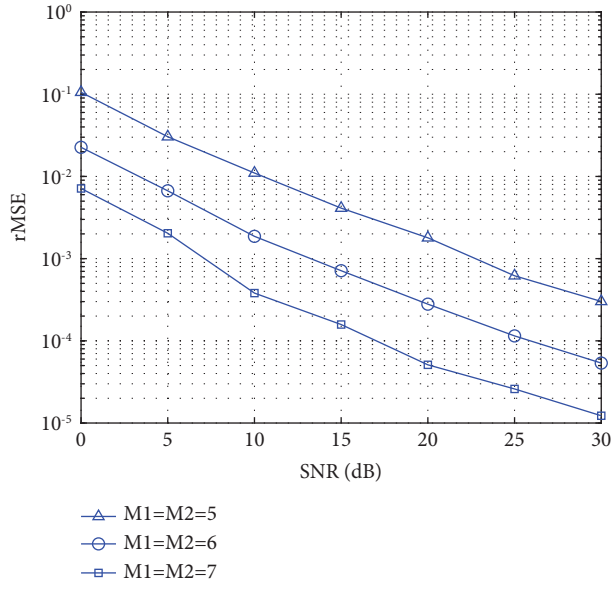

(b)

Figure 5: The rMSE performance with a different number of antennas. (a) $M_r = 4$. (b) $M_r = 8$.

The rMSEs of channel matrices are used to characterize the estimation performance [18, 19].

$\mathbf{X}$, $\mathbf{C}_1$, and $\mathbf{C}_3$ are set as discrete Fourier transform (DFT) matrices. For the first case in Figure 4, the number of antennas is set as $M_1 = M_2 = 4$, and $M_r = 3$, which satisfies the first case with $\mathbf{X} \in \mathbb{C}^{8\times 8}$. The factor matrices are $\mathbf{C}_1 = \mathbf{D}_3$, $\mathbf{C}_2 = \mathbf{I}_3$, and $\mathbf{C}_3 = \mathbf{D}_3$, where $\mathbf{D}_3 \in \mathbb{C}^{3\times 3}$ is the DFT matrix. As for the second case, the number of antennas is set as $M_1 = M_2 = 5$, $M_r = 8$, $\mathbf{X} \in \mathbb{C}^{10\times 10}$, and $\mathbf{C}_1 = \mathbf{D}_8$, $\mathbf{C}_2 = \mathbf{I}_8$, and $\mathbf{C}_3 = \mathbf{D}_8$, where $\mathbf{D}_8 \in \mathbb{C}^{8\times 8}$ is the DFT matrix. In Figures 4(a) and 4(b), we show the estimation accuracy of the channel and symbol in both cases. It is easy to see that the proposed method has lower rMSE and bit error rate (BER) compared with the least squares (LS) algorithm and MMSE algorithm under both conditions, and as the signal-to-noise ratio (SNR) value increases, the reductions in the rMSE and BER are observed.

Figures 5(a) and 5(b) show the influence when the number of antennas at the relays and the users is different. For the case in Figure 5(a), the number of relay antennas is set as $M_r = 4$, which satisfies $\{M_1, M_2\} \geqslant M_r$. For the case in Figure 5(b), the number of relay antennas is set as $M_r = 8$, which satisfies $\{M_1, M_2\} < M_r$. With the increasing number of users antennas, the spatial diversity gain increases, which improves the estimation accuracy and the rMSE performance of the algorithm gradually improve.

Figure 6 plots the complementary cumulative distribution function (CCDF) of the rMSE for a fixed SNR of 30 dB

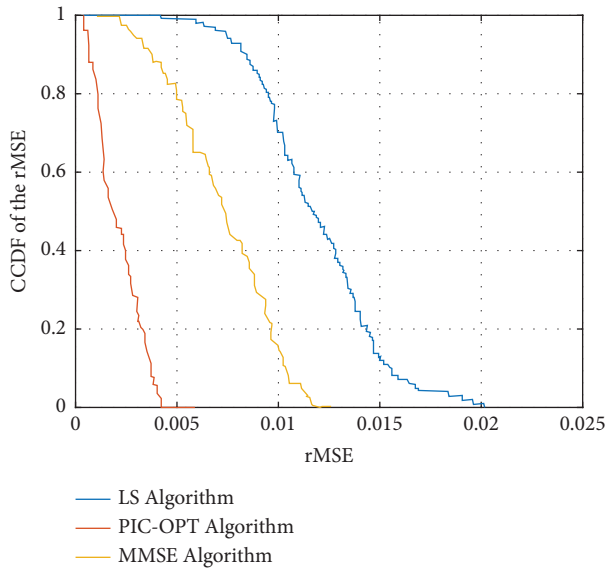

Figure 6: The CCDF performance of the PIC-OPT algorithm compared with that of the LS algorithm and the MMSE algorithm.

and randomly drawn channel realizations. The rMSE value of the proposed method is concentrated in the lower range than that of the LS algorithm and the MMSE algorithm.

6. Conclusion

In this paper, a PIC-OPT receiver based on the PARAFAC model of a two-way MIMO UAV-aided cooperative communication system is proposed. The simulation results show that compared with the traditional LS receiver, the proposed PIC-OPT receiver has better rMSE performance and BER performance. Our numerical results confirm the effectiveness of the proposed receiver. In addition, the application of this method in millimeter-wave MIMO systems is a prospect of this paper. Our work considers the PIC-OPT receiver in stationary scenarios, and the extended work including channel modeling and estimation in some high-mobility scenarios can be considered [20, 21].

Data Availability

The data used in this paper are provided by simulations and that the material used to support the findings of this study is available from the corresponding author upon request.

Conflicts of Interest

The authors declare that they have no conflicts of interest.

Acknowledgments

This work was supported in part by the Key Research and Development Program (No. 2020YFC0811004), NSFC under Grant 62001008, Beijing Municipal Natural Science Foundation under Grants 4212002 and L192034, Beijing Education Committee Project under Grant KM201910009011, Key Laboratory of Universal Wireless Communications Ministry of Education under Grant KFKT-2020104, and NCUT Startup Project.

References

[1] R. K. Ahiadormey, P. Anokye, H. S. Jo, and K. J. Lee, "Performance analysis of two-way relaying in cooperative power line communications," *IEEE Access*, vol. 7, pp. 97264–97280, 2019.

[2] F. Heliot and R. Tafazolli, "Optimal energy-efficient source and relay precoder design for two-way MIMO-AF relay systems," *IEEE Transactions on Green Communications and Networking*, vol. 4, no. 3, pp. 759–773, 2020.

[3] C. C. Hu and B. H. Chen, "Two-way MIMO relaying systems employing layered relay-and-antenna selection strategies," *IEEE Systems Journal*, vol. 12, no. 1, pp. 854–861, 2018.

[4] N. Ayir and P. Ubaidulla, "Transceiver design for MIMO full-duplex two-way relay network," *IEEE Wireless Communications Letters*, vol. 7, no. 5, pp. 772–775, 2018.

[5] T. Routtenberg and J. Tabrikian, "Blind MIMO-AR system identification and source separation with finite-alphabet," *IEEE Transactions on Signal Processing*, vol. 58, no. 3, pp. 990–1000, 2010.

[6] C. W. R. Chiong, Y. Rong, and Y. Xiang, "channel training algorithms for two-way MIMO relay systems," *IEEE Transactions on Signal Processing*, vol. 61, no. 16, pp. 3988–3998, 2013.

[7] F. Roemer and M. Haardt, "tensor-based channel estimation and iterative refinements for two-way relaying with multiple antennas and spatial reuse," *IEEE Transactions on Signal Processing*, vol. 58, no. 11, pp. 5720–5735, 2010.

[8] X. Han, X. Zhao, A. L. F. de Almeida, W. d. C. Freitas, and W. Bai, "Enhanced tensor-based joint channel and symbol estimation in dual-hop MIMO relaying systems," *IEEE Communications Letters*, vol. 25, no. 5, pp. 1655–1659, 2021.

[9] X. Han, Y. Zhao, and J. Ying, "Semi-blind receivers for UAV M-KRST coding MIMO systems based on nested tensor models," *IEEE Wireless Communications Letters*, vol. 10, no. 1, pp. 185–188, 2021.

[10] A. Johnson, J. Francis, B. Madathil, and S. N. George, "A two-way optimization framework for clustering of images using weighted tensor nuclear norm approximation," in *Proceedings of the 2020 National Conference on Communications (NCC)*, pp. 1–5, Kharagpur, India, April 2020.

[11] L. Hongbo, M. Jin, G. Songhu, and M. Junkai, "Identification and simulation of interference cancellation system self adaptive filtering," in *Proceedings of the 2018 37th Chinese Control Conference (CCC)*, pp. 1892–1897, Wuhan, China, July 2018.

[12] M. R. A. Khandaker and K. K. Wong, "Joint source and relay optimization for interference MIMO relay networks," *EURASIP Journal on Applied Signal Processing*, vol. 2017, no. 1, 2017.

[13] G. Liu, A. Liu, R. Zhang, and M. Zhao, "Angular-domain selective channel tracking and Doppler compensation for high-mobility mmWave massive MIMO," *IEEE Transactions on Wireless Communications*, vol. 20, no. 5, pp. 2902–2916, 2021.

[14] Z. Wang, Y. Cai, A. Liu, J. Wang, and G. Yue, "Mixed-timescale channel estimation for MIMO relay multi-user systems based on the PARAFAC decomposition," *IEEE Communications Letters*, vol. 25, no. 4, pp. 1288–1292, 2021.

[15] N. D. Sidiropoulos and R. S. Budampati, "Khatri-Rao space-time codes," *IEEE Transactions on Signal Processing*, vol. 50, no. 10, pp. 2396–2407, 2002.

[16] M. Haardt, F. Roemer, and G. Del Galdo, "Higher-order SVD-based subspace estimation to improve the parameter estimation accuracy in multidimensional harmonic retrieval problems," *IEEE Transactions on Signal Processing*, vol. 56, no. 7, pp. 3198–3213, 2008.

[17] X. Han, A. L. de Almeida, and Z. Yang, "Channel estimation for MIMO multi-relay systems using a tensor approach," *EURASIP Journal on Applied Signal Processing*, vol. 2014, pp. 163–214, 2014.

[18] H. Xi and A. L. F. de Almeida, "Multiuser receiver for joint symbol/channel estimation in dual-hop relaying systems," *Wireless Personal Communications*, vol. 83, no. 1, pp. 17–33, 2015.

[19] X. Han, Y. Zhou, X. Zhao, and W. Bai, "channel estimation method based on multi-way array in CCFD systems," *Journal of South China University of Technology*, vol. 48, no. 1, pp. 133–138, 2020.

[20] T. Zhou, Y. Yang, L. Liu, C. Tao, and Y. Liang, "A dynamic 3-D wideband GBSM for cooperative massive MIMO channels in intelligent high-speed railway communication systems," *IEEE Transactions on Wireless Communications*, vol. 20, no. 4, pp. 2237–2250, 2021.

[21] T. Zhou, C. Tao, S. Salous, and L. Liu, "Geometry-based multi-link channel modeling for high-speed train communication networks," *IEEE Transactions on Intelligent Transportation Systems*, vol. 21, no. 3, pp. 1229–1238, 2020.